

Reevaluation of the reported observation of the ${}_{\Lambda\Lambda}^4\text{H}$ hypernucleus

S. D. Randeniya and E. V. Hungerford

Department of Physics, University of Houston, Houston, Texas 77204, USA

(Received 11 June 2007; published 10 December 2007)

The results of experiment E906, undertaken at the Alternating Gradient Synchrotron of the Brookhaven National Laboratory (BNL-AGS), were reanalyzed to clarify the signature of the decays of the double- and single- Λ hypernuclei that could have been produced in this experiment. This reanalysis indicates that instead of the reported decay of ${}_{\Lambda\Lambda}^4\text{H}$ through a proposed resonance in ${}_{\Lambda}^4\text{He}$, it is more probable that the decay of the ${}_{\Lambda\Lambda}^7\text{He}$ hypernucleus was observed. This decay was accompanied by a background of coincident decays of pairs of the single hypernuclear fragments ${}_{\Lambda}^3\text{H}$ with ${}_{\Lambda}^4\text{H}$, ${}_{\Lambda}^3\text{H}$ with ${}_{\Lambda}^3\text{H}$, and ${}_{\Lambda}^4\text{H}$ with ${}_{\Lambda}^4\text{H}$. An attempt was also made to determine if any other double or coincident single hypernuclear species could be observed in the data.

DOI: [10.1103/PhysRevC.76.064308](https://doi.org/10.1103/PhysRevC.76.064308)

PACS number(s): 21.80.+a, 21.10.Dr, 21.60.Cs, 27.10.+h

I. INTRODUCTION

Ten years after the discovery of single- Λ hypernuclei [1], a double- Λ hypernuclear event was observed and reported in the literature [2]. To date, a total of four double- Λ hypernuclei have been reported in five experiments (Table I). These events were analyzed to extract the binding energies of the Λ hyperons. With the exception of the experiment to be discussed below, all were single-event observations, and in one case the identity of the hypernucleus was not uniquely determined [4]. Two of these experiments [3,7] report the observation of the ${}_{\Lambda\Lambda}^6\text{He}$ hypernucleus but extract very different binding energies (10.9 MeV [3] as opposed to 7.25 MeV [7]). In addition, the interpretation of the results of the counter experiment [8] to be discussed below required an “unusual” decay mode to match the experimental data.

However, many double Λ hypernuclei are certainly stable with respect to decay via the strong interaction, and the analysis of double- Λ binding energies has been the subject of many recent discussions [9,10]. The binding of double- Λ hyperons to a nucleus can be used to determine the strength of the Λ - Λ potential and in particular to refine the $\text{SU}(3)_f$ baryon-baryon potential. It also affects the stability of the H dibaryon [11] and the composition of cold, dense nuclear matter, e.g., neutron stars [12].

The older set of double Λ events support a strongly interacting $\Lambda\Lambda$ system [11]; one that, in fact, might even produce a bound $\Lambda\Lambda$ state. The newer ${}_{\Lambda\Lambda}^6\text{He}$ event [7] indicates that the interpretation of the earlier observation of this hypernucleus was erroneous. Subsequent reanalysis of all the double hypernuclear events, after replacing the earlier measurement with the more recent one, provide a $\Lambda\Lambda$ binding energy that is consistent with a weak interaction potential. This later interaction is so weak that a stable ${}_{\Lambda\Lambda}^4\text{H}$ hypernucleus may not exist [13,14]. However, the weak form of the $\Lambda\Lambda$ interaction is reproduced by the NSC97 Nijmegen model [15], although other Nijmegen models cover a range of possibilities.

Because it is crucially important to understand multistrange nuclei and no new data will be available for some time, we have reinvestigated the published results of the BNL experiment E906. This counter experiment [8] reported the observation of the ${}_{\Lambda\Lambda}^4\text{H}$ hypernucleus by measuring the sequential pionic

decays after a (K^-, K^+) reaction deposited two units of strangeness in a ${}^9\text{Be}$ target. However, it is unfortunate that now only the published data are available for this reanalysis.

II. THE E906 EXPERIMENT

Experiment E906 was completed at the Alternating Gradient Synchrotron (AGS) of the Brookhaven National Laboratory (BNL). It used a momentum analyzed, 1.8-GeV K^- beam, incident on a ${}^9\text{Be}$ target. The target was placed at the center of a cylindrical detection system, CDS, containing tracking chambers and scintillators inside an axial magnetic field. Positive kaons from a (K^-, K^+) reaction were observed by a magnetic spectrometer behind the CDS.

The reaction was ${}^9\text{Be}(K^-, K^+)X$, where the missing mass, X , was selected to be a nuclear system containing two units of strangeness. The experimental analysis applied a missing mass cut that removed many quasi-free Ξ hyperons to reduce background. The recoiling system is therefore assumed to break up into nuclear fragments containing two Λ particles, in which none, one, or both of the Λ s could be bound to a fragment. All hyperfragments range in the target before they decay, and their identity is determined by the spectroscopy of their coincident mesonic decay as observed in the CDS. Tracking, pulse height, and timing provided particle identification.

A hypernucleus decays by the weak interaction either by emission of a pion (mesonic decay) or by the strangeness-changing weak interaction, $\Lambda N \rightarrow NN$ (nonmesonic decay). For hypernuclei with $A > 5$, nonmesonic decay becomes increasingly important as the momentum of the recoil nucleon in the mesonic decay, $\Lambda \rightarrow \pi^- N$, is below the nuclear Fermi surface. Therefore, the probability of mesonic decay decreases but that of nonmesonic decay increases, roughly keeping the hypernuclear lifetime at an approximate 200 ps. Mesonic decay can result in a two- or three-body decay process, and in the case of a two-body decay, the emitted pion from an at-rest system will have a precise momentum that can be used to determine the identity of a decaying hypernucleus. For example, a decay sequence for a double hyperfragment,

TABLE I. Observed $\Lambda\Lambda$ hypernuclei.

Hypernucleus	Detection	Ref.
${}_{\Lambda\Lambda}^{10}\text{Be}$	Emulsion	[2]
${}_{\Lambda\Lambda}^6\text{He}$	Emulsion	[3]
${}_{\Lambda\Lambda}^{10}\text{Be}$; or	Emulsion	[4]
${}_{\Lambda\Lambda}^{13}\text{B}$	Emulsion	[5,6]
${}_{\Lambda\Lambda}^6\text{He}$	Hybrid/Emulsion	[7]
${}_{\Lambda\Lambda}^4\text{H}$	Counter	[8]

${}_{\Lambda\Lambda}^A Y$, could be

$$\begin{aligned} {}_{\Lambda\Lambda}^A Y(Z, N) &\rightarrow \pi + {}_{\Lambda}^A Y'(Z+1, N) \\ &\rightarrow \pi + \pi + {}^A R(Z+2, N). \end{aligned}$$

A useful quantity, $\Delta B_{\Lambda\Lambda}$, is defined by the equations

$$\text{mass}({}_{\Lambda\Lambda}^A Y) = \text{mass}({}^{A-2}R') + 2 \text{mass}(\Lambda) - B_{\Lambda\Lambda}$$

$$\Delta B_{\Lambda\Lambda} = B_{\Lambda\Lambda} - 2B_{\Lambda}({}^{A-1}Y).$$

Thus $\Delta B_{\Lambda\Lambda}$ represents the additional binding energy due to the interaction of the two Λ s in the nucleus. This comes from a direct $\Lambda\Lambda$ interaction as well as indirectly by alteration of the nuclear core.

The two-dimensional, coincident pion spectrum obtained in Experiment 906 is shown in Figure 1. In this figure the higher of the two pion momenta, p_h , is plotted on the vertical axis and the lower, p_l , on the horizontal axis. It is important to recognize that this folds the spectrum about the line $p_h = p_l$ and any enhancements near this edge will be narrowed due to the folding of the spectrum back on itself. In the figure, the

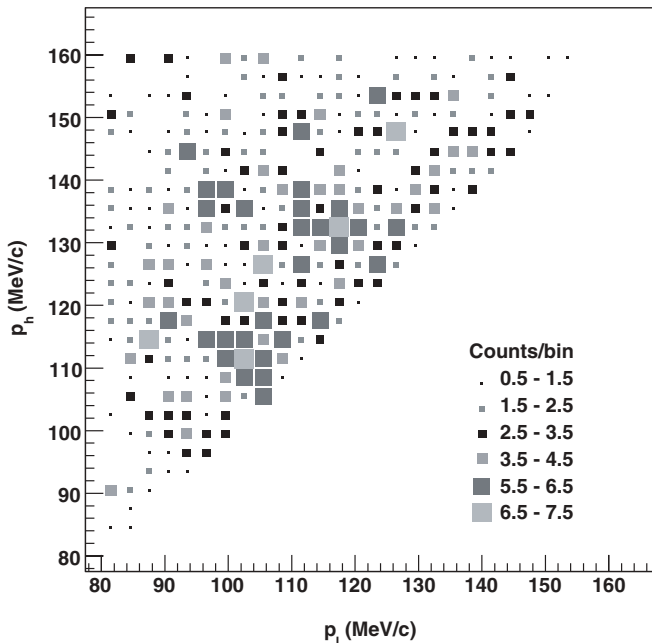


FIG. 1. The coincident pion spectrum emitted in the reaction ${}^9\text{Be}(K^-, K^+)X$ [8].

box size represents the number of the observed events in a two-dimensional momentum bin.

The figure shows several regions of enhanced counts. Region 1, positioned near pion momenta (114,132) MeV/c, is identified as due to the coincident decay of two single hypernuclei, ${}_{\Lambda}^3\text{H}$ and ${}_{\Lambda}^4\text{H}$, as it has the correct pion momenta for these decays. However, the discussion in this article mainly involves the interpretation of the enhancement at pion momenta near (105,115) MeV/c, region 2, and perhaps other possible enhancements around pion momenta (98,137) MeV/c, region 3, and below 107 MeV/c.

To explain the data in region 2, the published E906 analysis invoked a resonant state [16] in the ${}_{\Lambda}^4\text{He}$ system. Thus the pion decays were presumed to proceed as

$$\begin{aligned} {}_{\Lambda\Lambda}^4\text{H} &\rightarrow \pi + {}_{\Lambda}^4\text{He}^*(8.9) \rightarrow \pi + p + {}_{\Lambda}^3\text{H} \\ &\rightarrow \pi + p + \pi + {}^3\text{He}. \end{aligned}$$

The ${}_{\Lambda}^4\text{He}^*$ resonance assignment was arbitrary, and selected to match the observed pion energies. It was required to be narrow so that the ${}_{\Lambda\Lambda}^4\text{H} \rightarrow \pi + {}_{\Lambda}^4\text{He}^*(8.9)$ decay produces a more-or-less monoenergetic pion. However, there is no other evidence for such a state, and it is unlikely that a narrow, resonant structure this high in excitation energy in this hypernuclear nuclear system would exist. Therefore, we have undertaken a detailed simulation of all possible pion decays from appropriate at-rest hypernuclear systems to investigate whether these observations might be explained more conventionally.

III. DESCRIPTION OF THE MONTE CARLO SIMULATION

A. Pion decays

To identify the sequential decays that could be produced from various single- and double-hypernuclear species a Monte Carlo simulation was developed that includes all possible mesonic decays from various hypernuclei that could be produced by the ${}^9\text{Be}(K^-, K^+)X$ reaction. The simulation includes decays to two-body as well as three-body final states, and decays to and from excited as well as ground states. We have used the newer, weak value of $\Delta B_{\Lambda\Lambda}$ (Table II) to fix the masses of the double-hypernuclear systems. This value

TABLE II. Estimated values of $\Delta B_{\Lambda\Lambda}$. The older value [11] of $\Delta B_{\Lambda\Lambda} \approx 2.5\text{--}3.0$ MeV should be compared to the values in this table.

${}_{\Lambda\Lambda}^B A$	$B_{\Lambda}(A-1)$	$B_{\Lambda\Lambda}$	$\Delta B_{\Lambda\Lambda}$	$M_{\Lambda\Lambda}(A)$	Ref.
${}_{\Lambda\Lambda}^4\text{H}$	0.13	Unbound		4107.48	[13]
${}_{\Lambda\Lambda}^4\text{He}$	0.056	0.107		4107.37	[14]
${}_{\Lambda\Lambda}^5\text{H}$	2.04	3.26	0.82	5037.54	[10]
${}_{\Lambda\Lambda}^5\text{He}$	2.39	3.80	0.98	5036.98	[10,17]
${}_{\Lambda\Lambda}^6\text{He}$	3.12	7.25	1.01	5952.52	Exp. [7]
${}_{\Lambda\Lambda}^6\text{He}$	3.12	10.94	4.7	5948.83	Exp. [3]
${}_{\Lambda\Lambda}^7\text{He}$	4.18	9.36	(1.0)	6890.86	[6]

of $\Delta B_{\Lambda\Lambda}$ is consistent with the new analysis of $\Lambda\Lambda$ binding energies, as explained in Sec. I above. For the simulation, pion spectra presented in several references were used [18–29]. Natural decay widths were used for the three-body decay spectra as obtained directly from the spectra in the published references and the spectra were spread by the quoted standard deviation of the momentum resolution of the CDS, 4 MeV/c.

The (K^-, K^+) reaction could proceed by the production of a Ξ^- that then produces a $\Lambda\Lambda$ hypernucleus through Ξ^- capture on another nucleus in the target. However, given the momentum transfer in this reaction, a Ξ recoil would most often decay in flight or range at a distance greater than the 2-cm cut at the reaction vertex. Thus, production of recoil systems containing two units of strangeness should primarily occur through a direct, two-step process on a single target nucleus. The (K^-, K^+) reaction on a ^9Be target, changes two protons into two Λ s, so the recoiling nuclear medium is composed of two protons, two Λ s, and five neutrons. These could produce the double hypernuclear species, assuming at least one neutron is emitted to bring the system to equilibrium, ${}_{\Lambda\Lambda}^8\text{He}$, ${}_{\Lambda\Lambda}^7\text{He}$, ${}_{\Lambda\Lambda}^6\text{He}$, ${}_{\Lambda\Lambda}^5\text{He}$, ${}_{\Lambda\Lambda}^5\text{H}$, and ${}_{\Lambda\Lambda}^4\text{H}$. The reaction can also produce combinations of quasi-free Λ s, and the various single- Λ hypernuclei, ${}_{\Lambda}^7\text{He}$, ${}_{\Lambda}^6\text{He}$, ${}_{\Lambda}^5\text{He}$, ${}_{\Lambda}^4\text{He}$, ${}_{\Lambda}^5\text{H}$, ${}_{\Lambda}^4\text{H}$, and ${}_{\Lambda}^3\text{H}$. While hyperfragments of single- Λ systems could form, the reaction must conserve baryon number and charge. Thus, for example, the simultaneous production of ${}_{\Lambda}^4\text{H}$ and ${}_{\Lambda}^4\text{H}$ is possible, but the production of ${}_{\Lambda}^4\text{He}$ and ${}_{\Lambda}^3\text{H}$ is not. The experiment required the detection of two, time-coincident pionic decays, and the double Λ systems, ${}_{\Lambda\Lambda}^5\text{H}$, ${}_{\Lambda\Lambda}^6\text{He}$, and ${}_{\Lambda\Lambda}^7\text{He}$ were predicted to be most copiously produced (Table III). The formation probabilities calculated in Table III used the older, larger value for the $\Lambda\Lambda$ potential, $\Delta B_{\Lambda\Lambda} \approx 4$ MeV.

Once formed, the double hypernuclei range and transition to their ground states. They then either decay by mesonic or nonmesonic emission. In principle, the production reaction or the decay could involve isomeric levels from which weak decay could occur; however, no excited states in double-hypernuclear systems for $A \leq 6$ are expected [6,23]. Also only mesonic decay is observed in this experiment.

Pionic emission in hypernuclear weak decays can leave the residual nucleus or hypernucleus in an excited as well as its ground state. In addition, decays can originate from excited states, if these various nuclear levels are isomeric. As

TABLE III. Theoretical formation probabilities of double hypernuclei in a two-step (K^-, K^+) reaction on a ^9Be target [18].

Hypernucleus	Formation probability
${}_{\Lambda\Lambda}^4\text{H}$	0.02
${}_{\Lambda\Lambda}^5\text{H}$	0.40
${}_{\Lambda\Lambda}^5\text{He}$	0.006
${}_{\Lambda\Lambda}^6\text{He}$	0.080
${}_{\Lambda\Lambda}^7\text{He}$	0.098

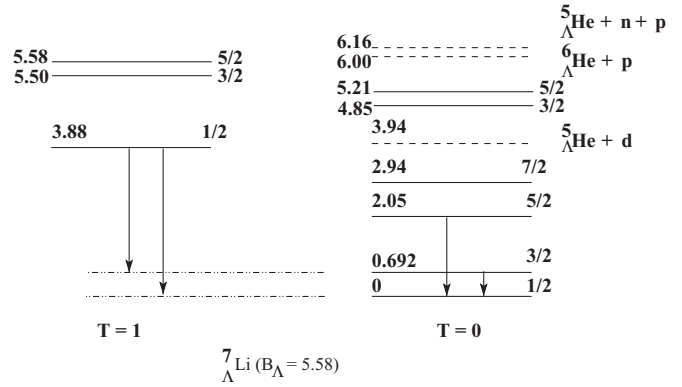


FIG. 2. The level structure and gamma transitions in ${}_{\Lambda}^7\text{Li}$.

an example pertinent to discussions below, Figure 2 shows the level structure of ${}_{\Lambda}^7\text{Li}$. This hypernucleus and its excited states are produced in the mesonic decay of ${}_{\Lambda\Lambda}^7\text{He}$. De-excitation from the excited states occurs by γ emission or by weak decay if the γ lifetime is sufficiently retarded. Table IV gives the calculated probability of decays from various levels in ${}_{\Lambda}^7\text{Li}$. These are determined using the weak decay lifetime $\Gamma = 200$ ps and the electromagnetic transition times of the various levels obtained from the calculation of Ref. [24]. One sees that $\approx 96\%$ of the decay is expected to occur in the ground state, and although decay from excited states is included in our simulation, this effect is negligible.

B. Background

The experimental background is expected to come from decays of quasi-free Ξ^- s, quasi-free Λ s, and quasi-free Λ s associated with hypernuclear decays. Because the Λ s are uncharged they will always decay in flight. Therefore, the experiment attempted to discriminate against background by requiring a vertex cut of 2 cm obtained by back-tracking the directions of the observed pions. For a Λ to move ≤ 2 cm within a mean life, its momentum must be ≤ 293 MeV/c. Of course the Λ could be moving in any direction when it decays, and within the Λ center-of-mass the pion is emitted uniformly in all directions. Thus the pion momentum is boosted and could have a value up to ≈ 150 MeV/c. Therefore one would expect that pions more-or-less uniformly populate the momentum bins in the region of interest, perhaps decreasing above 140 MeV/c

TABLE IV. Probability of weak decay from various levels in ${}_{\Lambda}^7\text{Li}$.

Level	Probability
5/2 (5.58)	1.5×10^{-6}
3/2 (5.50)	5.5×10^{-7}
1/2 (4.1)	1.5×10^{-7}
7/2 (2.94)	1.7×10^{-3}
5/2 (2.05)	3.3×10^{-2}
3/2 (0.69)	1.4×10^{-3}
1/2 (0.00)	1.0

or so. Certainly the background should be slowly varying and one does not expect structure. Indeed the background quasi-free decay spectra, as was presented in Ref. [8] are approximately constant. Therefore, given the statistical precision of the data, we apply a simple background model that is constant up to the spectrum edges and decreases as a Gaussian with a decay factor equal to the bin width [1.5 MeV/c (FWHM)] at the $p_h = p_l$ limit. Finally, we note that data above a pion momentum of 140 MeV/c are found to have a constant five/counts per two-dimensional momentum bin. Although the background is assumed constant in our simulation, its strength is varied to minimize a fit to the data as explained below.

IV. FITS TO THE DATA

The published data, in addition to the two-dimensional plot of coincident pion momentum, Figure 1, provided two pairs of one-dimensional pion spectra, projected on the momentum axis of one of the pions when the momentum of other pion lay within a selected window. We attempt to fit these projected spectra by our simulation, although we note that the statistical precision of the data and the experimental resolution are poor, and the experimental cross sections are not available. A best fit to each pair of the one-dimensional projections is obtained by optimizing the normalization constants using a χ^2 minimization procedure that equally weighted the two projections for each pair; i.e., projections I and II and then III and IV, as obtained from the published article. The errors on each data point were taken as the square root of the number of counts in that momentum bin. Certainly the actual error associated with each data point is larger than this and increasing the error will simply improve the χ^2 of the fit. However, no other information was available for this analysis to account for the error more accurately.

A. Branching ratios and decay spectra

According to the enhancements seen in Figure 1, hypernuclei that could have been potentially seen in the experiment are ${}^4_{\Lambda}\text{H}$, ${}^3_{\Lambda}\text{H}$ (region 1), ${}^8_{\Lambda\Lambda}\text{He}$, ${}^7_{\Lambda\Lambda}\text{He}$ (region 2), ${}^5_{\Lambda\Lambda}\text{H}$ (region 3) and ${}^6_{\Lambda\Lambda}\text{He}$. The ${}^4_{\Lambda\Lambda}\text{H}$ hypernucleus was not included in this analysis as it required the unusual decay mode to fit the experimental data, and it is not clear if this system is actually bound [10,15].

This analysis used decay spectra from experimental data whenever it was available. For all the $\Lambda\Lambda$ hypernuclei only theoretical estimates were available, and for this analysis pion spectra given in Ref. [18] were used. For ${}^4_{\Lambda}\text{H}$ and ${}^3_{\Lambda}\text{H}$ hypernuclei several theoretical and experimental studies were found (Table V). Two experimental studies were found for the ${}^3_{\Lambda}\text{H}$ hypernucleus [22,27] and one [22] provided an experimentally measured mesonic decay spectrum that was used for the analysis. The two-body and three-body decay spectra of this hypernucleus overlap due to small binding energy (0.13 MeV) and the experimental energy resolution. Although the decay rates given in the references do not agree, this effect is minimal.

For the ${}^4_{\Lambda}\text{H}$ hypernucleus no experimentally measured full pion spectrum was found. Several articles present only the

TABLE V. Branching ratios for the mesonic decays of ${}^3_{\Lambda}\text{H}$ and ${}^4_{\Lambda}\text{H}$ hypernuclei taken from several references.

Hypernucleus	Reference	Two-body	Three-body
${}^3_{\Lambda}\text{H}$	[18]	0.34	0.19
${}^3_{\Lambda}\text{H}$	[22](Exp.)	26	47
${}^3_{\Lambda}\text{H}$	[27](Exp.)	127	150
${}^4_{\Lambda}\text{H}$	[18]	0.42	0.30
${}^4_{\Lambda}\text{H}$	[26]	0.618	0.271
${}^4_{\Lambda}\text{H}$	[19]	0.525	0.252
${}^4_{\Lambda}\text{H}$	[27](Exp.)	914	401

continuum spectrum [28,29] and branching ratios [27,30]. Two theoretically calculated pion spectra were also available [18, 26]. Both of these gave roughly the same value for the three-body decay width but differ in two-body strength. However the ratio of three-body to two-body decay widths of Ref. [26] agree well with the experimentally measured value. The shape of the continuum spectrum is almost the same in both spectra and quite similar to the experimental curve.

We employed both decay spectra in the analysis to see if the uncertainties in the branching ratios make any difference in the final results. In the following sections fits to different spectral regions are discussed. Schemes 1 and 2 correspond to the cases in which the ${}^4_{\Lambda}\text{H}$ decay spectrum was taken from Refs. [18] and [26], respectively.

B. Fit to projections III and IV

In projections III and IV the enhancement is expected to be essentially due to the coincident decay of ${}^4_{\Lambda}\text{H}$ with ${}^3_{\Lambda}\text{H}$. The simulation in this region included two- and three-body decays of ${}^4_{\Lambda}\text{H}$ and ${}^3_{\Lambda}\text{H}$ hypernuclei, the possible decay of ${}^5_{\Lambda\Lambda}\text{H}$, and a constant background. The fit to data using scheme 2 is shown in Fig. 3. For scheme 1 histograms are essentially the same, and therefore not shown in the figure. The χ^2 of the fit is ~ 1 per degree of freedom for both schemes (Table VI). The decay sequences and the normalizations of ${}^4_{\Lambda}\text{H}$ and ${}^3_{\Lambda}\text{H}$ hypernuclei are summarized in Table VII. The normalization for the quasi-free background obtained from this fit was ≈ 0.02 for 25,000 Monte Carlo throws and was kept constant throughout the analysis to maintain the consistency between different spectral regions.

TABLE VI. The χ^2 per degree of freedom for the local fits, the global fit, and the global representation using schemes 1 and 2.

Projection	Scheme 1	Scheme 2
I/II	0.804	0.922
III/IV	0.959	0.898
Global fit	1.31	2.06
Global rep.	1.35	2.08

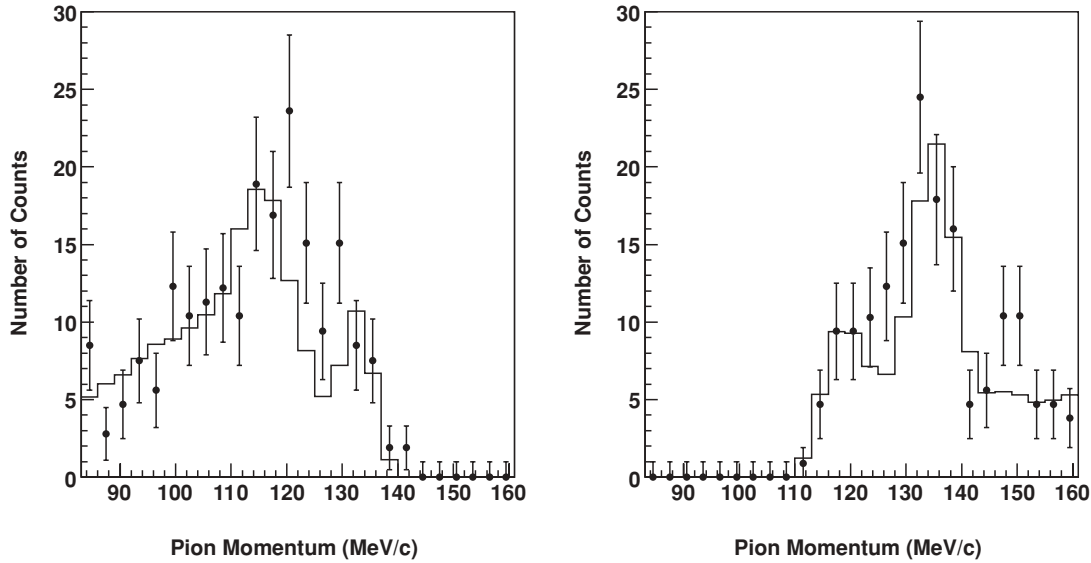


FIG. 3. The projected pion spectra for the coincident pion decays comparing the simulation (histogram) to the data (points with errors) using scheme 2. The left figure shows the projection onto the p_l (IV) axis and the right the p_h axis (III).

The hypernucleus, ${}_{\Lambda\Lambda}^5\text{H}$, was then included in the simulation as it could potentially add strength in the momentum region (98,138) MeV/c. However, it was rejected by the minimization procedure as the normalization become negative in both schemes. Therefore the fit to the data is insensitive to the decay of the ${}_{\Lambda\Lambda}^5\text{H}$ system. However, the coincident decay of ${}_{\Lambda}^4\text{H}$ (two-body) with ${}_{\Lambda}^4\text{H}$ (three-body), does improve the fit. Contribution from ${}_{\Lambda}^3\text{H}$ - ${}_{\Lambda}^3\text{H}$ coincident decay is very small compared to ${}_{\Lambda}^4\text{H}$ - ${}_{\Lambda}^4\text{H}$ coincident decay, but this also improves the fit. Both of these single- Λ hypernuclear decays reduced the χ^2 about 0.59 per degree of freedom when added to the ${}_{\Lambda}^4\text{H}$ - ${}_{\Lambda}^3\text{H}$ coincidence spectrum.

Therefore, the data is consistent with the coincident decay of ${}_{\Lambda}^4\text{H}$ and ${}_{\Lambda}^3\text{H}$ added to a small constant background of five to six counts per two-dimensional momentum bin, plus the decay of the two single hypernuclear pairs ${}_{\Lambda}^4\text{H}$ with ${}_{\Lambda}^4\text{H}$ and ${}_{\Lambda}^3\text{H}$ with ${}_{\Lambda}^3\text{H}$.

C. Fit to projections I and II

The simulation in this region included the decay of the ${}_{\Lambda\Lambda}^7\text{He}$ hypernucleus. In addition, the coincident decay of the three pairs of single hypernuclei and the constant background

TABLE VII. Normalizations obtained from the local fits for each hypernuclear decay mode along with the number of Monte Carlo throws.

Decay mode	Scheme 1	Scheme 2	MC throws
${}_{\Lambda\Lambda}^7\text{He}$	0.005043	0.005847	10900
${}_{\Lambda}^3\text{H}/{}_{\Lambda}^4\text{H}$	0.002361	0.001975	45000
${}_{\Lambda}^3\text{H}/{}_{\Lambda}^3\text{H}$	0.000597	0.000754	45000
${}_{\Lambda}^4\text{H}/{}_{\Lambda}^4\text{H}$	0.002330	0.001194	45000

that were determined from the previous fit were included. The three-body decay of the single-hypernuclear pairs add strength in the region of interest and must be included. As an example see Fig. 4. The fit to experimental data using scheme 2 is shown in Fig. 5 where the χ^2 of the fit is ~ 1 per degree of freedom (Table VI).

The effect on χ^2 when the decay of ${}_{\Lambda\Lambda}^6\text{He}$ was included was examined. This hypernucleus does not have a two-body π^- decay channel. In the three-body decay of this system into a pion, a proton, and a ${}_{\Lambda}^5\text{He}$ system, the cut-off pion momentum is about 102 MeV/c. Because the momentum resolution of the CDS is 4 MeV/c, the ${}_{\Lambda\Lambda}^6\text{He}$ decay spectrum could perhaps add background in the projections I and II (Fig. 6).

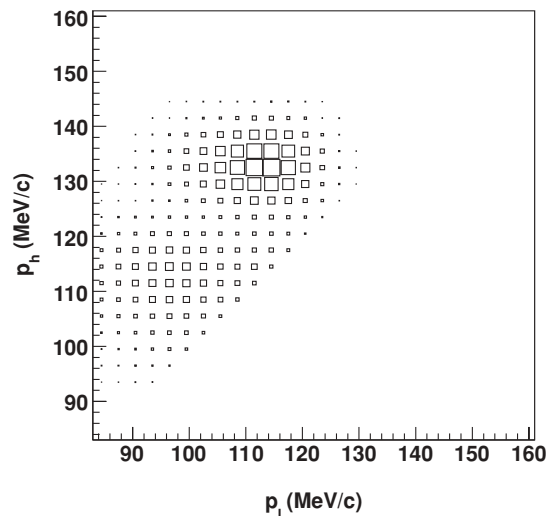


FIG. 4. The two-dimensional pion decays from simultaneously produced hypernuclei ${}_{\Lambda}^3\text{H}$ and ${}_{\Lambda}^4\text{H}$. Note not only the two-body ground state, but three-body decays are included.

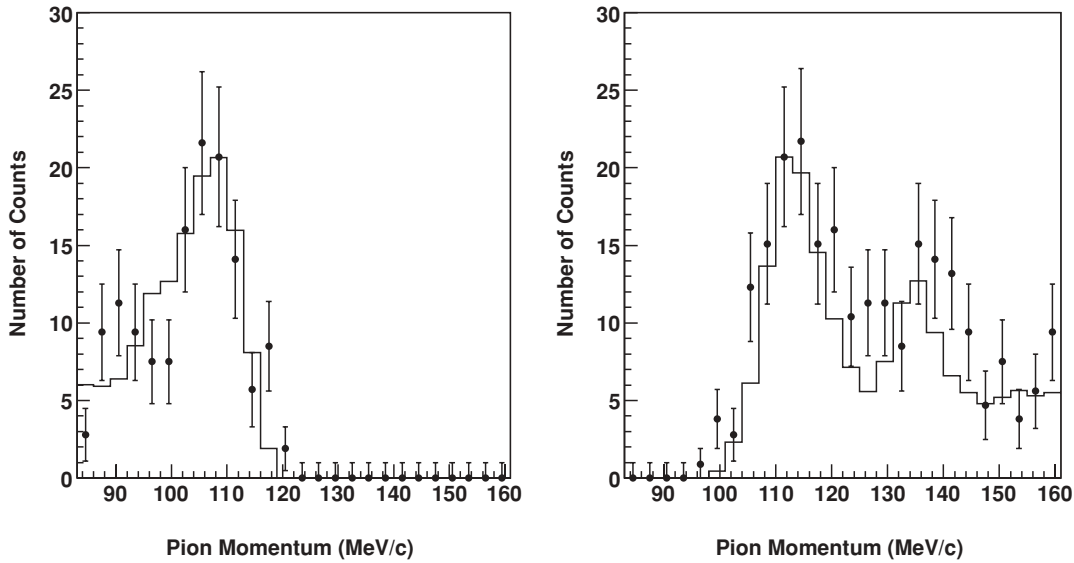


FIG. 5. The projected pion spectra for the coincident pion decays comparing the simulation (histogram) to the data (points with errors). The left figure shows the projection onto the p_l (II) axis and the right the p_h axis (I).

However, the χ^2 of the fit essentially did not change when the decay of this hypernucleus was included in both schemes. However, the normalization corresponding to the ${}_{\Lambda\Lambda}^7\text{He}$ decay was reduced as the normalization for ${}_{\Lambda\Lambda}^6\text{He}$ increased. Hence up to the minimum χ^2 value, the inclusion of the ${}_{\Lambda\Lambda}^6\text{He}$ decay balances the counts removed from the ${}_{\Lambda\Lambda}^7\text{He}$ decay, and the data in this region are insensitive to the inclusion of the ${}_{\Lambda\Lambda}^6\text{He}$ hypernucleus. Decay from the ${}_{\Lambda\Lambda}^5\text{He}$ hypernuclei were not included in this fit as this decay essentially overlaps the ${}_{\Lambda\Lambda}^6\text{He}$ decay spectrum and thus its strength is effectively included in the ${}_{\Lambda\Lambda}^6\text{He}$ analysis.

In summary, the data can be represented by the decay of ${}_{\Lambda\Lambda}^7\text{He}$ along with decay of three single hypernuclear pairs, ${}_{\Lambda}^4\text{H}$ with ${}_{\Lambda}^4\text{H}$ and ${}_{\Lambda}^3\text{H}$ with ${}_{\Lambda}^3\text{H}$ and ${}_{\Lambda}^3\text{H}$ with ${}_{\Lambda}^4\text{H}$ and a constant

background as described above. Table VII summarizes the normalizations obtained from the two local fits.

D. Production of ${}_{\Lambda\Lambda}^6\text{He}$ hypernuclei

Most of the counts in the ${}_{\Lambda\Lambda}^6\text{He}$ decay spectrum appear in the region below $p_h = 107 \text{ MeV}/c$ and the decay of ${}_{\Lambda\Lambda}^7\text{He}$ adds background in this region, Figure 6.

A fit of the simulation to the projected experimental data in the region where $92 \text{ MeV}/c \leq p_h \leq 107 \text{ MeV}/c$ and $86 \text{ MeV}/c \leq p_l \leq 98 \text{ MeV}/c$, keeping the normalizations determined from previous fits constant and including the decay of ${}_{\Lambda\Lambda}^6\text{He}$, is shown in Fig. 7. The χ^2 of the fit is 67 for 51 degrees of freedom, whereas the background from all the hypernuclear

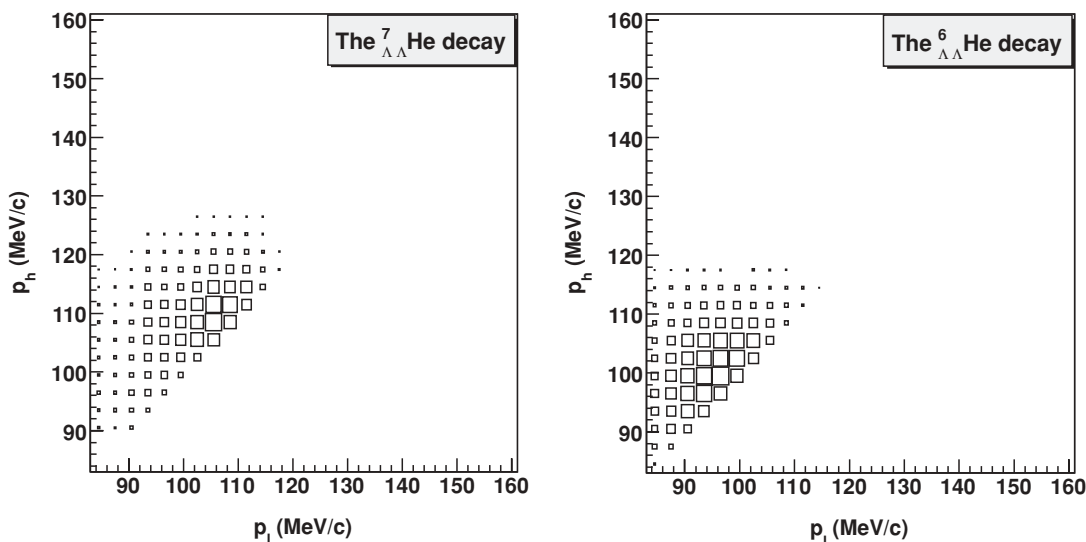


FIG. 6. The two-dimensional pion decays from the decay of ${}_{\Lambda\Lambda}^7\text{He}$ and ${}_{\Lambda\Lambda}^6\text{He}$ hypernuclei.

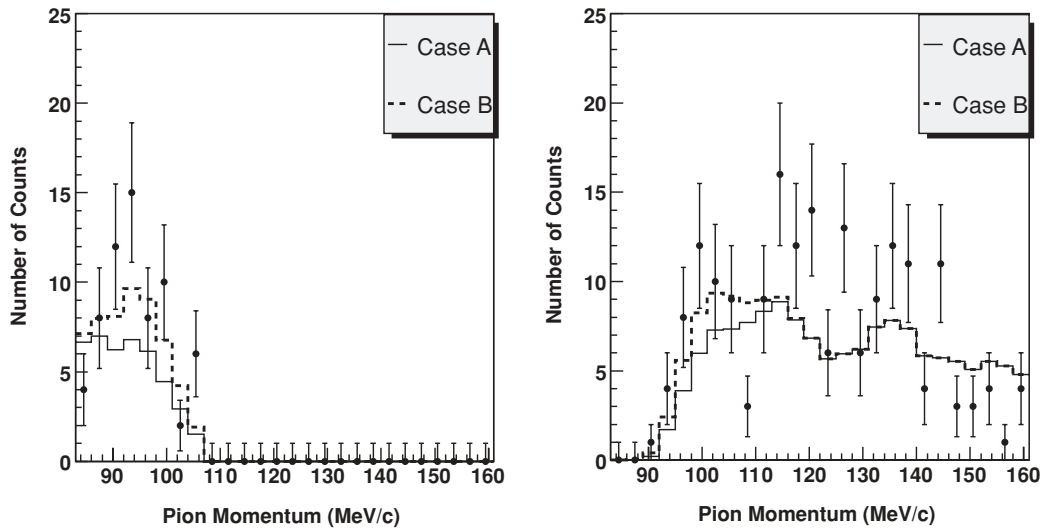


FIG. 7. The projected pion spectra for the coincident pion decays comparing the simulation (histograms) to the data (points with errors). The left figure shows the projection onto the p_l axis and the right onto the p_h axis. The solid histogram represent the background due to the decay of ${}_{\Lambda\Lambda}^7\text{He}$, single hypernuclear pairs and a constant background. The dashed histogram shows all of the above plus the inclusion of ${}_{\Lambda\Lambda}^6\text{He}$ decay.

decays previously discussed plus the constant background alone give a χ^2 of 73 for 52 degrees of freedom. However, the data in the projection onto p_l axis seem to be well represented when the decay from the ${}_{\Lambda\Lambda}^6\text{He}$ system is included while similar behavior is observed in the momentum region between 90 MeV/c and 110 MeV/c, when projected onto p_h axis. Unfortunately, the statistical change in the fit cannot confirm the observation of this hypernucleus.

E. Global picture

A comparison of a global fit to the experimental data, keeping the normalizations of the local fits and including all

the regions described above, is shown in Fig. 8. This includes the decay of ${}_{\Lambda\Lambda}^7\text{He}$ along with the three single hypernuclear pairs and the constant background. The projection onto p_l axis corresponds to events that have p_h between 101 and 143 MeV/c, and the projection on to p_h axis corresponds to events that have p_l between 92 and 137 MeV/c. The χ^2 calculated using this analysis is 70 for the 52 degrees of freedom, using scheme 1. Using scheme 2, this is about 108 for 52 degrees of freedom. Although the χ^2 of scheme 2 is higher, the peaks fit fairly well in both schemes. The valleys seem to lose counts going from scheme 1 to scheme 2 when the data are projected onto p_h axis. Counts in the valleys of the spectral region depend on the shape of the ${}_{\Lambda}^4\text{H}$ decay spectrum.

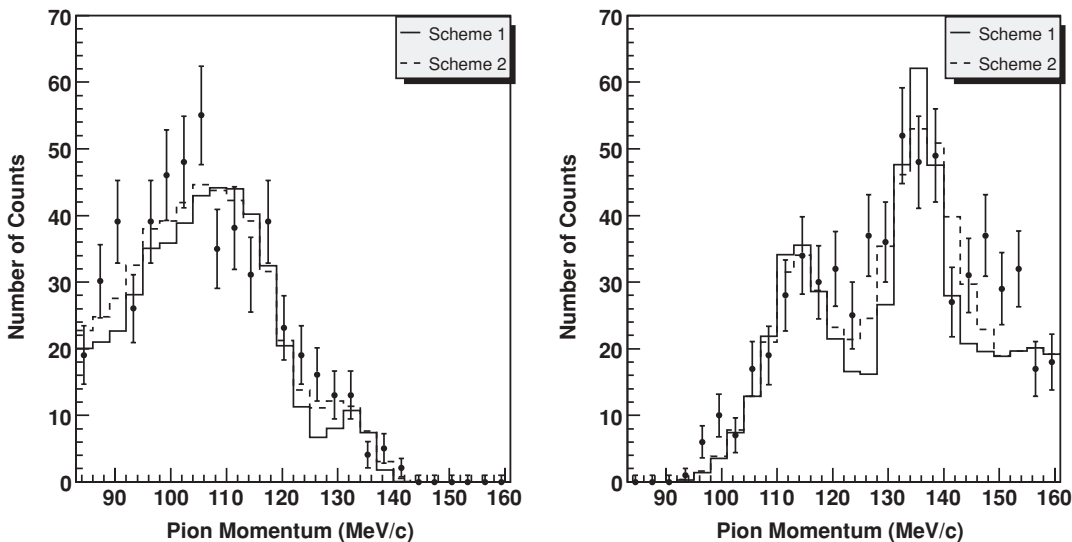


FIG. 8. The projected pion spectra for the coincident pion decays comparing the simulation (histograms) to the data (points with errors). Solid histogram: scheme 1, dashed histogram: scheme 2. The left figure shows the projection onto the p_l axis and the right, the p_h axis.

TABLE VIII. Normalizations obtained from the global fit for each hypernuclear decay mode along with the number of Monte Carlo throws.

Decay mode	Scheme 1	Scheme 2	MC throws
${}_{\Lambda\Lambda}^7\text{He}$	0.005963	0.007830	10900
${}_{\Lambda}^3\text{H}/{}_{\Lambda}^4\text{H}$	0.003423	0.003064	45000
${}_{\Lambda}^3\text{H}/{}_{\Lambda}^3\text{H}$	0.000160	0.000121	45000
${}_{\Lambda}^4\text{H}/{}_{\Lambda}^4\text{H}$	0.002466	0.000970	45000

Inclusion of ${}_{\Lambda\Lambda}^6\text{He}$ essentially does not change the χ^2 of the simulation fit to the data.

If the normalizations were allowed to vary, the same simulation gives a minimum χ^2 of 63 for 48 degrees of freedom using scheme 1, and 99 for 48 degrees of freedom for scheme 2 (Table VI). The histograms essentially overlap with those in Fig. 8 for both schemes. Figures 9 and 10 show how the simulation fit to data improves when the background and different single hypernuclear pairs are included. Table VIII summarizes the normalizations obtained from this global fit. They are statistically close to the values from the local fits (Table VII). Inclusion of ${}_{\Lambda\Lambda}^6\text{He}$ into the fit shows the same behavior discussed in the fit to regions I and II. One finds for this case that the coincident decay of ${}_{\Lambda}^3\text{H}$ with ${}_{\Lambda}^3\text{H}$ is not necessarily needed to obtain the best fit. This is a problem caused by overlap of the pion spectra in the region of interest,

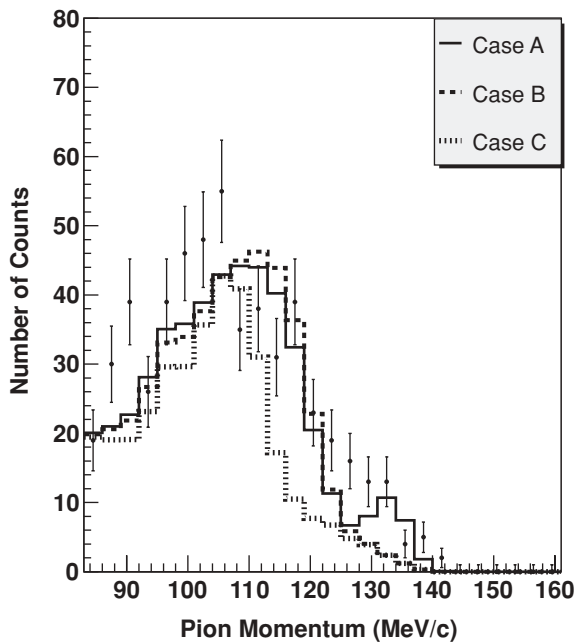


FIG. 9. The coincident pion spectrum projected on to p_l axis comparing the simulation (histograms) to the data (points with errors) using scheme 2. Case A corresponds to the simulation fit of the ${}_{\Lambda\Lambda}^7\text{He}$ spectrum combined with all the single hypernuclear pairs plus a constant background. Case B includes ${}_{\Lambda\Lambda}^7\text{He}$, coincident ${}_{\Lambda}^3\text{H}-{}_{\Lambda}^4\text{H}$ and the background. Case C includes ${}_{\Lambda\Lambda}^7\text{He}$ added to the constant background.

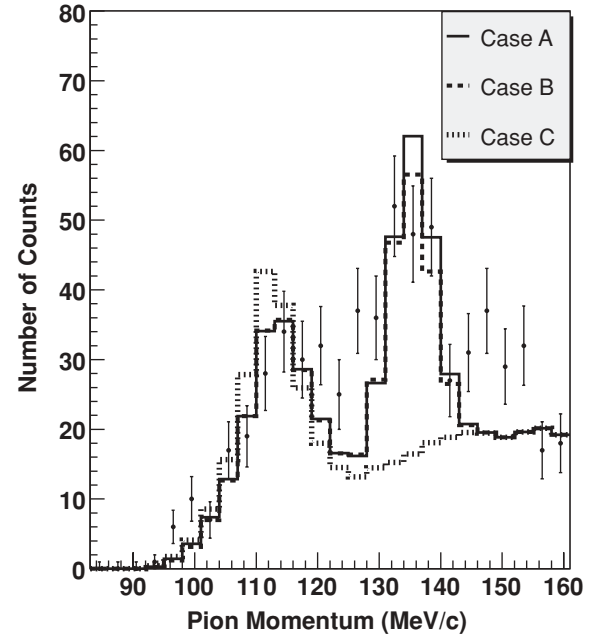


FIG. 10. The coincident pion spectrum projected on to p_h axis comparing the simulation (histograms) to the data (points with errors) using scheme 2. Case A corresponds to the simulation fit of the ${}_{\Lambda\Lambda}^7\text{He}$ spectrum combined with all the single hypernuclear pairs plus a constant background. Case B includes ${}_{\Lambda\Lambda}^7\text{He}$, coincident ${}_{\Lambda}^3\text{H}-{}_{\Lambda}^4\text{H}$ and the background. Case C includes ${}_{\Lambda\Lambda}^7\text{He}$ added to a constant background.

as the number of counts from one decay spectrum can be compensated by another decay spectrum when projected onto p_l and p_h axes in the global fit. For example, in the projection onto the p_l axis, in the global fit, both ${}_{\Lambda}^3\text{H}-{}_{\Lambda}^3\text{H}$ coincident decay and ${}_{\Lambda}^4\text{H}-{}_{\Lambda}^4\text{H}$ coincident decay add counts between 110 and 120 MeV/c. Similarly, for the projection onto the p_h axis, ${}_{\Lambda\Lambda}^7\text{He}$ decay and ${}_{\Lambda}^3\text{H}-{}_{\Lambda}^3\text{H}$ coincident decay add counts in the momentum region between 110 and 120 MeV/c. This leads to an increase in the number of counts from ${}_{\Lambda}^3\text{H}-{}_{\Lambda}^4\text{H}$ and ${}_{\Lambda\Lambda}^7\text{He}$ coincident decays and a decrease in counts from ${}_{\Lambda}^3\text{H}-{}_{\Lambda}^3\text{H}$ coincident decay.

This overlap is not that severe in projections III and IV as each spectrum adds counts in more isolated momentum regions. However, in projections I and II several decay spectra overlap, such as the decay of ${}_{\Lambda\Lambda}^7\text{He}$ with the decay of three single hypernuclear pairs as discussed above. Because the normalizations for these single hypernuclear pairs were determined from the fit to projections III and IV, most of the complications arising from the overlap were removed, but the amount of background obtained in the fit affects the number of counts from the ${}_{\Lambda\Lambda}^7\text{He}$ decay.

In general, overlap of decay spectra can lead to misinterpretation of data. As an example, an independent fit to projections I and II produces a minimum χ^2 when the decay of ${}_{\Lambda\Lambda}^5\text{H}$ is included, in addition to ${}_{\Lambda\Lambda}^7\text{He}$ and coincident ${}_{\Lambda}^3\text{H}-{}_{\Lambda}^3\text{H}$ decay, but with removal of ${}_{\Lambda}^4\text{H}-{}_{\Lambda}^4\text{H}$ coincidence decay. However, keeping the normalizations determined from this fit constant, a fit to projections III and IV (region 1), including ${}_{\Lambda}^3\text{H}-{}_{\Lambda}^4\text{H}$ coincident decay, gives a $\chi^2 \approx 2$, higher than the

TABLE IX. Branching ratios for the ${}^3_{\Lambda}\text{H}$ hypernucleus. For scheme 1 values are taken from Ref. [18] and for scheme 2 experimental values are used [22,32–34].

Decay mode	Scheme 1	Scheme 2
${}^3_{\Lambda}\text{H} \rightarrow {}^3\text{He} + \pi^-$	0.34	0.222
${}^3_{\Lambda}\text{H} \rightarrow d + p + \pi^-$	0.18	0.412
${}^3_{\Lambda}\text{H} \rightarrow {}^3\text{H} + \pi^0$	0.17	0.111
${}^3_{\Lambda}\text{H} \rightarrow d + n + \pi^0$	0.10	0.206
Γ_{NM}	0.21	0.049
Γ_{Total}	1.00	1.00

previously discussed value for this region. Therefore, the decay spectra must be combined carefully to extract the decay sequences.

V. PRODUCTION RATIO

In both schemes the ${}^7_{\Lambda\Lambda}\text{He}$ decay spectrum presented in Ref. [18] was used. In that calculation, the ${}^7_{\Lambda\Lambda}\text{He} \rightarrow {}^7_{\Lambda}\text{Li} + \pi^-$ decay rate is 0.26 of the free Λ decay rate and the ${}^7_{\Lambda}\text{Li} \rightarrow {}^7\text{Be} + \pi^-$ decay rate is 24% of the total decay rate. The total mesonic decay rate is 0.78 of the free Λ decay rate. The nonmesonic decay rate was assumed to be 50% of the total decay rate following reference [31]. Given this information the two-body decay rate of ${}^7_{\Lambda\Lambda}\text{He}$ is about 4% of the total decay rate.

Branching ratios for the ${}^3_{\Lambda}\text{H}$ and ${}^4_{\Lambda}\text{H}$ hypernuclei are given in Tables IX and X, respectively. Experimental branching ratios for the ${}^4_{\Lambda}\text{H}$ hypernucleus were taken from Ref. [30]. For the ${}^3_{\Lambda}\text{H}$, the two-body π^- decay width was obtained from Ref. [32] as the mean value of several experimental reports [22,33]. The nonmesonic decay width was taken as 0.049 following Ref. [34]. Other decay rates were interpolated following the $\Delta I = \frac{1}{2}$ rule [35].

According to scheme 1, the number of coincident ${}^3_{\Lambda}\text{H}$ - ${}^4_{\Lambda}\text{H}$ events corresponding to two-body decay, as extracted from the fit is about 19 counts and that of ${}^7_{\Lambda\Lambda}\text{He}$ is about 48 counts, and the production ratio of ${}^7_{\Lambda\Lambda}\text{He}$ to coincident ${}^3_{\Lambda}\text{H}$ - ${}^4_{\Lambda}\text{H}$

TABLE X. Branching ratios for the ${}^4_{\Lambda}\text{H}$ hypernucleus. For scheme 1 values are taken from Ref. [18] and for scheme 2 experimental values are used [30].

Decay mode	Scheme 1	Scheme 2
${}^4_{\Lambda}\text{H} \rightarrow {}^4\text{He} + \pi^-$	0.36	0.51
${}^4_{\Lambda}\text{H} \rightarrow {}^3\text{H} + p + \pi^-$	0.26	0.23
No two-body	N/A	N/A
${}^4_{\Lambda}\text{H} \rightarrow {}^3\text{H} + n + \pi^0$	0.13	0.12
Γ_{NM}	0.25	0.13
Γ_{Total}	1.00	1.00

is about 7.7, producing about 1200 ${}^7_{\Lambda\Lambda}\text{He}$ events in the experiment.

Using the experimental branching ratios, coincident ${}^3_{\Lambda}\text{H}$ - ${}^4_{\Lambda}\text{H}$ two-body events obtained from the fit is 13 and that of ${}^7_{\Lambda\Lambda}\text{He}$ is 57. This gives a production ratio of 12, which is about 1400 ${}^7_{\Lambda\Lambda}\text{He}$ events for the experiment.

The production ratios presented here are different from what was presented in Ref. [36], as this analysis was extended to include possible production of ${}^6_{\Lambda\Lambda}\text{He}$ and effects due to uncertainty in the branching ratios of the single- Λ hypernuclei as discussed above.

VI. CONCLUSIONS

Our analysis shows that published E906 data can be represented without the inclusion of ${}^4_{\Lambda\Lambda}\text{H}$ decay. It is more likely that the decay of ${}^7_{\Lambda\Lambda}\text{He}$ was observed in this experiment along with a background of three single hypernuclear pairs. Whether the ${}^4_{\Lambda\Lambda}\text{H}$ system is bound remains an open question, but its formation and decay were not needed to explain these data. The analysis is consistent with the assignment of a weak value for $\Delta B_{\Lambda\Lambda}$, and for ${}^7_{\Lambda\Lambda}\text{He}$ this is ~ 1 MeV.

Although the inclusion of decays from coincident ${}^3_{\Lambda}\text{H}$ with ${}^3_{\Lambda}\text{H}$ and ${}^4_{\Lambda}\text{H}$ with ${}^4_{\Lambda}\text{H}$ reduces the χ^2 of the simulation fit to the data, the statistical significance is poor.

Ref. [18] calculates the production of double- and single- Λ species from the ${}^9\text{Be}(K^-, K^+)$ reaction assuming a Ξ^- interacts with another ${}^9\text{Be}$ nucleus. The production probabilities presented in this reference use a value of $\Delta B_{\Lambda\Lambda} \approx 4$ MeV, which as explained above, is consistent with the older value of the Λ - Λ interaction potential. Although this article states that calculations were also made with $\Delta B_{\Lambda\Lambda} = 0$ MeV, only the total production distribution ratios between quasi-free Λ , twin Λ hypernuclear, and double- Λ hypernuclear production are given. These predict that ${}^5_{\Lambda\Lambda}\text{H}$ would be the lightest hypernucleus produced. However, within the statistical sensitivity of the experiment no evidence was found for the production of ${}^5_{\Lambda\Lambda}\text{H}$ hypernuclei. Absence of ${}^5_{\Lambda\Lambda}\text{H}$ in the data perhaps indicates that this system is unbound or weakly bound. There is some evidence for the production of the ${}^6_{\Lambda\Lambda}\text{He}$ hypernucleus.

Reference [18] also assumes that the production process proceeds through an intermediate, compound state that then emits Λ s, nucleons, or fissions into hypernuclear pairs. So the (K^-, K^+) reaction may have produced ${}^8_{\Lambda\Lambda}\text{He} + n$. However, a simulation of the decay of ${}^8_{\Lambda\Lambda}\text{He}$ does not change the conclusions of this analysis. The ${}^8_{\Lambda\Lambda}\text{He}$ hypernucleus does not have two-body decays in either of the π^- decay sequences, making it difficult to identify.

Extremely good energy resolution and some type of particle identification of the decaying system are necessary if this experimental technique is to be used in future studies. It is important to overcome confusion when decay spectra overlap, especially the backgrounds coming from coincident single hypernuclear pairs in the regions of interest. In addition, much better vertex reconstruction would help reduce quasi-free backgrounds, requiring extremely good tracking resolution.

- [1] M. Danysz and J. Pniewski, *Phil. Mag.* **44**, 348 (1958).
- [2] M. Danysz *et al.*, *Phys. Rev. Lett.* **11**, 29 (1963).
- [3] D. J. Prowse, *Phys. Rev. Lett.* **17**, 782 (1966).
- [4] S. Aoki *et al.*, *Prog. Theor. Phys.* **85**, 1287 (1991).
- [5] C. B. Dover *et al.*, *Phys. Rev. C* **44**, 1905 (1991).
- [6] E. Hiyama *et al.*, *Nucl. Phys.* **A754**, 103c (2005).
- [7] H. Takahashi *et al.*, *Phys. Rev. Lett.* **87**, 212502 (2001).
- [8] J. K. Ahn *et al.*, *Phys. Rev. Lett.* **87**, 132504 (2001).
- [9] C. Albertus, J. E. Amaro, and J. Nieves, *Phys. Rev. Lett.* **89**, 032501 (2002); H. Nemura *et al.*, *Nucl. Phys.* **754**, 110c (2005).
- [10] A. Gal, *Nucl. Phys.* **A754**, 91c (2005).
- [11] R. H. Dalitz *et al.*, *Proc. R. Soc. London A* **426**, 1 (1989); T. Yamada, *Nucl. Phys.* **A691**, 250 (2001).
- [12] D. Blaschke, N. K. Glendenning, and A. Sedrakian, eds., *Lecture Notes in Physics: Physics of Neutron Star Interiors* (Springer Verlag, Berlin, 2001), Vol. 578.
- [13] I. N. Filikhin and A. Gal, *Phys. Rev. Lett.* **89**, 172502 (2002).
- [14] H. Nemura, Y. Akaishi, and K. S. Myint, *Phys. Rev. C* **67**, 051001(R) (2003).
- [15] Th. A. Rijken, *Nucl. Phys.* **A691**, 322c (2001); Th. A. Rijken and Y. Yamamoto, *ibid.* **A754**, 27c (2005); V. G. J. Stoks and Th. A. Rijken, *Phys. Rev. C* **59**, 3009 (1999); Th. A. Rijken, V. G. J. Stoks and Y. Yamamoto, *Phys. Rev. C* **59**, 21 (1999); Th. A. Rijken, *Phys. Rev. C* **73**, 044007 (2006); Th. A. Rijken and Y. Yamamoto, *Phys. Rev. C* **73**, 044008 (2006).
- [16] D. E. Kahana, S. H. Kahana, and D. J. Millener, *Phys. Rev. C* **68**, 037302 (2003).
- [17] I. N. Filikhin, A. Gal, and V. M. Suslov, *Phys. Rev. C* **68**, 024002 (2003).
- [18] Y. Yamamoto *et al.*, *Nucl. Phys.* **A625**, 107 (1997).
- [19] T. Motoba *et al.*, *Nucl. Phys.* **A534**, 597 (1991).
- [20] T. Motoba, K. Itonga, and H. Bando, *Nucl. Phys.* **A489**, 683 (1988).
- [21] T. Fukuda *et al.*, *Phys. Rev. C* **58**, 1306 (1998).
- [22] G. Keyes *et al.*, *Phys. Rev. D* **01**, 66 (1969).
- [23] E. Hiyama, M. Kamimura, T. Motoba, T. Yamada, and Y. Yamamoto *et al.*, *Phys. Rev. C* **66**, 024007 (2002).
- [24] E. Hiyama, M. Kamimura, K. Miyazaki, and T. Motoba, *Phys. Rev. C* **59**, 2351 (1999).
- [25] H. Kamada, J. Golak, K. Miyagawa, H. Witala, and W. Glockle, *Phys. Rev. C* **57**, 1595 (1998).
- [26] I. Kumagai-Fuse, S. Okabe, and Y. Akaishi, *Phys. Rev. C* **54**, 2843 (1996).
- [27] D. Bertrand *et al.*, *Nucl. Phys.* **B16**, 77 (1969).
- [28] U. Krecker *et al.*, *Nucl. Phys.* **A236**, 491 (1974).
- [29] O. Adamovič *et al.*, *Lett. Nuovo Cimento* **6**, 09 (1973).
- [30] H. Ota *et al.*, *Nucl. Phys.* **A639**, 251c (1998).
- [31] K. Itonaga *et al.*, *Mod. Phys. Lett. A* **18**, 135 (2003).
- [32] J. G. Congleton *et al.*, *J. Phys. G: Nucl. Part. Phys.* **18**, 339 (1992).
- [33] G. Keyes *et al.*, *Phys. Rev. Lett.* **20**, 819 (1968); *Nucl. Phys.* **B67**, 269 (1973).
- [34] C. Benhold, A. Ramos, D. A. Aruliah, and U. Oelfke, *Phys. Rev. C* **45**, 947 (1991).
- [35] E. D. Commins and P. H. Bucksbaum, *Weak Interactions of Leptons and Quarks* (Cambridge University Press, London, 1983).
- [36] S. D. Randeniya and E. V. Hungerford, Proceedings of the IX International Conference on Hypernuclear and Strange Particle Physics, 2006 (to be published).